General Disclaimer

One or more of the Following Statements may affect this Document

- This document has been reproduced from the best copy furnished by the organizational source. It is being released in the interest of making available as much information as possible.

- This document may contain data, which exceeds the sheet parameters. It was furnished in this condition by the organizational source and is the best copy available.

- This document may contain tone-on-tone or color graphs, charts and/or pictures, which have been reproduced in black and white.

- This document is paginated as submitted by the original source.

- Portions of this document are not fully legible due to the historical nature of some of the material. However, it is the best reproduction available from the original submission.

NASA Technical Memorandum 87032

Fast Approach for Calculating Film Thicknesses and Pressures in Elastohydrodynamically Lubricated Contacts at High Loads

Luc G. Houpert and Bernard J. Hamrock
Lewis Research Center
Cleveland, Ohio

Prepared for the
Joint Lubrication Conference
cosponsored by the American Society of Lubrication Engineers
and the American Society of Mechanical Engineers
Atlanta, Georgia, October 8–10, 1985

NASA

FAST APPROACH FOR CALCULATING FILM THICKNESSES AND PRESSURES IN ELASTOHYDRODYNAMICALLY LUBRICATED CONTACTS AT HIGH LOADS

Luc G. Houpert* and Bernard J. Hamrock
National Aeronautics and Space Administration
Lewis Research Center
Cleveland, Ohio 44135

SUMMARY

The film thicknesses and pressures in elastohydrodynamically lubricated contacts have been calculated for a line contact by using an improved version of Okamura's approach. The new approach allows for lubricant compressibility, the use of Roelands' viscosity, a general mesh (nonconstant step), and accurate calculations of the elastic deformations. The new approach is described, and the effects on film thickness, pressure, and pressure spike of each of the improvements are discussed. Successful runs have been obtained at high pressure (to 4.8 GPa) with low CPU times.

SYMBOLS

a_{ij} weighting factors used to define dP/dX at node i

b half Hertzian length, $R\sqrt{8W/\pi}$, m

C_j weighting factors used to integrate P

D_{ij} influence coefficient used to calculate elastic deformation at node i due to P_j

E Young's modulus of surface, Pa

E' equivalent Young's modulus, $\frac{1}{E'} = \frac{1}{2}\left(\frac{1 - \nu_a^2}{E_a} + \frac{1 - \nu_b^2}{E_b}\right)$, Pa

G materials parameter, $\alpha E'$

H dimensionless film thickness, $hR/b^2 = \pi h/8RW$

H_e dimensionless film thickness where $dP/dX = 0$

H_0 dimensionless constant used in calculation of H

ΔH maximum deviation from flat shape of Hertzian contact

h film thickness, m

*Presently at S.K.F. Engineering and Research Center, 3430AB Nieuwegein, The Netherlands; NRC-NASA Research Associate during academic year 1984-85.

i,j	nodes
N	number of nodes used in linear system
N_{max}	maximum number of nodes used in mesh
P	dimensionless pressure, p/p_H, Pa
P_s	dimensionless pressure at spike
p	pressure
p_H	maximum Hertzian pressure, $E'b/4R = E'\sqrt{W/2\pi}$, Pa
R	equivalent radius of contact, m
r	radius of surface, m
U	dimensionless speed parameter, $\eta_0 u/E'R$
u	tangential speed of surface, m/s
u	average entrainment rolling speed, $(u_a + u_b)/2$, m/s
W	dimensionless load parameter, $w/E'R$
w	applied load per unit length, N/m
X	dimensionless abscissa, x/b
X_{end}	outlet meniscus distance
X_{max}	maximum value of X in mesh
X_{min}	minimum value of X in mesh, X_1
ΔX	constant step, $(X_N - X_1)/(N - 1)$, used in uniform mesh
x	abscissa along rolling direction, m
Z	Roelands' parameter
α	piezoviscous coefficient, m^2/N
$\bar{\delta}_H$	maximum dimensionless Hertzian deformation
δ_i	elastic deformation at node i, m
$\bar{\delta}_i$	dimensionless elastic deformation, $R\delta/b^2$
η_0	viscosity at operating temperature and ambient pressure, N s/m^2
ν	Poisson's ratio

$\bar{\rho}$ relative density

$\bar{\rho}_e$ relative density where $H = H_e$

Subscripts:

a surface a

B Barus

b surface b

H Hertz

i at node number i

j at node number j

max maximum value

min minimum value

R Roelands

INTRODUCTION

Elastohydrodynamic lubrication is a form of fluid-film lubrication where elastic deformations of the lubricated surfaces become significant. It is usually associated with highly stressed machine elements such as rolling-element bearings and gears. The first attempt to analyze elastohydrodynamically lubricated contacts was made by Grubin and Vinogradova (ref. 1), who managed to incorporate both the effects of elastic deformation and the viscosity-pressure characteristics of the lubricant in an inlet analysis of hydrodynamic lubrication of nonconformal contacts. Solutions to the coupled Reynolds and elasticity equations have proved to be difficult. An attempt to review the methods of obtaining numerical solutions to the elastohydrodynamic lubrication problem is presented by Hamrock and Tripp (ref. 2). Highlights of four main approaches are presented, namely the direct method, the inverse method, the quasi-inverse method, and the system approach method. The advantages and disadvantages of each method are discussed. As described by Hamrock and Jacobson (ref. 3), the direct method used a large amount of CPU time and the approach failed at high loads. (Maximum dimensionless load W was of the order of 3×10^{-5}).

A recently developed approach not covered in Hamrock and Tripp's review (ref. 2) is that of Okamura (ref. 4). Okamura uses a Newton-Raphson method to solve the elastohydrodynamic lubrication problem in a system form. Iterations on the system approach are still required, as was the case in the direct method; however, much less computer time is used. Furthermore, the major advantage of the method is that solutions can be obtained for higher loads than by the direct method. (Maximum dimensionless load W was of the order of 8×10^{-5}.) Nevertheless, these loads are much lower than those in rolling-element bearings, where W reaches the order of 1×10^{-3}. At high loads the

elastic deformations are several orders of magnitude larger than the film thickness. Any inaccuracy in the pressure will cause (via elasticity calculations) drastic changes in the film thickness that will in turn (via the Reynolds equation) cause large pressure fluctuations and numerical instabilities, especially when the viscosity is large, as is the case in normal EHL contacts. At high loads the viscosity of the fluid can vary by 10 orders of magnitude within the conjunction.

In the current study it was felt that the only way of solving the EHL problem at high loads was to accurately calculate the elastic deformations and the pressure gradient dP/dX, especially in the inlet region and near the pressure spike, where dP/dX is large. To calculate the pressure gradient, a general mesh (i.e., nonconstant step) is needed (a fine step when dP/dX is large). Okamura's method (ref. 4) was therefore extended to include these improvements.

For a comparable change in pressure the relative density change is considerably smaller than the viscosity change. The maximum density increase is about 35 percent. However, although the density effect is much smaller than the viscosity effect, the very high pressures in EHL films are such that the liquid should no longer be considered incompressible. Furthermore, high-pressure viscosity measurements have shown that Barus' expression cannot be used at high loads. A more realistic pressure-viscosity relationship as proposed by Roelands (ref. 5), should be used. Although Roelands expression is valid for pressures not exceeding 1 GPa, it can be used in EHL calculations at larger maximum pressures because the film thickness is mainly dependent on the inlet of the contact, where pressures are small. Therefore, lubricant compressibility and Roelands' viscosity were also introduced in the present approach. Different means (including the authors' new approach) of calculating the elastic deformations are first compared. After having described the new mathematical formulation, the effects on film thickness, pressure, and pressure spike of the mesh and number of nodes are studied in detail. Results are shown for low, intermediate, high, and very high loads. Finally results obtained using Barus' and Roelands' viscosity as well as the compressible and incompressible relationships are compared.

The authors wish to thank Dr. J. Tripp of the NASA Lewis Research Center and Mr. T. Lubrecht of the University of Twente, The Netherlands, who took part in many helpful discussions on the subject.

CALCULATION OF ELASTIC DEFORMATIONS

The elastic deformation δ at any point x on the surface is expressed as

$$\delta = -\frac{2}{\pi E'} \int_{x_{min}}^{x_{end}} p \ln (x - x')^2 \, dx' \tag{1}$$

where p is the pressure function of x', with x' varying between x_{min} and x_{end}. Letting $X = x/b$, $P = p/p_H$, $\bar{\delta} = R\delta/b^2$ where

$1/R = 1/R_a + 1/R_b$, $R/b = \sqrt{\pi/8W}$, $W = w/E'R$, and $p_H = E'b/4R$ gives

$$\bar{\delta} = -\frac{1}{2\pi}\left[\int_{X_{min}}^{X_{end}} P \ln (X - X')^2 \, dX' + \ln\left(R^2 \frac{8W}{\pi}\right) \int_{X_{min}}^{X_{end}} P \, dX'\right] \tag{2}$$

But $w = \int p \, dx$ implies $\int P \, dX' = \pi/2$. Making use of this, equation (2) becomes

$$\bar{\delta} = -\frac{1}{2\pi} \int_{X_{min}}^{X_{end}} P \ln (X - X')^2 \, dX' - \frac{1}{4} \ln\left(R^2 \frac{8W}{\pi}\right) \tag{3}$$

The constant term on the right side of equation (3) represents in general 80 to 90 percent of the total deformation. This is a very useful separation in that it puts the remaining pressure-dependent deformation of the same order as the film thickness at moderate loads. Using integration by parts on the integral gives

$$\bar{\delta} = -\frac{1}{2\pi} \left|PI\right|_{X_{min}}^{X_{end}} + \frac{1}{2\pi} \int_{X_{min}}^{X_{end}} \frac{dP}{dX'} \, I \, dX' - \frac{1}{4} \ln\left(R^2 \frac{8W}{\pi}\right) \tag{4}$$

where

$$I = \int \ln (X - X')^2 \, dX' = -(X - X') \left[\ln (X - X')^2 - 2\right] \tag{5}$$

Since the pressure is zero at X_{min} and X_{end}, we can write that

$$\bar{\delta} = -\frac{1}{2\pi} \int_{X_{min}}^{X_{end}} \frac{dP}{dX'} (X - X') \left[\ln (X - X')^2 - 2\right] dX' - \frac{1}{4} \ln\left(R^2 \frac{8W}{\pi}\right) \tag{6}$$

The integral in equation (6) can be calculated analytically by assuming that the pressure is described by a polynomial of second degree in the interval $[X_{j-1}, X_{j+1}]$. The details of the calculations are given in appendix A. The deformation $\bar{\delta}_i$ at node i is calculated as a function of the pressure P_j and the influence coefficients D_{ij}:

$$\bar{\delta}_i = \sum_{j=1}^{N} D_{ij} P_j - \frac{1}{4} \ln\left(R^2 \frac{8W}{\pi}\right) \tag{7}$$

The results obtained will be compared in table I with the ones obtained by Hamrock and Jacobson (ref. 2) and Okamura (ref. 4), who used simpler approaches. Hamrock and Jacobson assumed the pressure to be constant in the interval $[X_j - \Delta X/2, X_j + \Delta X/2]$ and used an analytical expression for the integral of $\log (X_i - X')$. Okamura did not use any analytical solutions and assumed simply that

$$\bar{\delta}_i = -\frac{1}{2\pi} \sum_{j=1}^{N} P_j \ln\left(\left|\frac{X_{i+1} + X_i}{2} - X_j\right| \left|\frac{X_{i-1} + X_i}{2} - X_j\right|\right) \tag{8}$$

The three approaches can be compared by assuming a Hertzian pressure. Between abscissa -1 and +1, the Hertzian shape should be flat, leading to $\Delta H = 0$ where ΔH is defined as

$$\Delta H = \frac{X^2}{2} + \bar{\delta} - \bar{\delta}_{max} \tag{9}$$

and $\bar{\delta}_{max}$ is the maximum deformation and can be compared with the Hertzian analytical value $\bar{\delta}_H$:

$$\bar{\delta}_H = -\frac{1}{4} \ln\left(R^2 \frac{8W}{\pi}\right) + \frac{1}{2} \ln(2) + 0.25 \tag{10}$$

The largest value $\Delta H_{max}/H_e$ of $\Delta H/H_e$ is found at abscissa $X = -1$ and $+1$ (because of the slope discontinuity) and is shown on table I with the corresponding value of $\bar{\delta}_{max}/\bar{\delta}_H - 1$. The central film thickness H_e has been chosen to be equal to 0.5; X_{min} and X_{max} define the first and last values of X; N_{max} is the number of nodes.

TABLE I. - THREE WAYS OF CALCULATING ELASTIC DEFORMATIONS

[OK: Okamura (ref. 4); HJ: Hamrock and Jacobson (ref. 3).]

N_{max}	X_{min}	X_{max}	$(\bar{\delta}_{max}/\bar{\delta}_H - 1)$			$\Delta H_{max}/H_e$		
			OK	HJ	New approach	OK	HJ	New approach
51	-1.0	1.0	-1.9×10^{-3}	-2.7×10^{-3}	8.6×10^{-7}	9.4×10^{-3}	-5.5×10^{-3}	-2.7×10^{-3}
51	-3.6	1.4	-4.9×10^{-3}	-1.1×10^{-2}	1.0×10^{-5}	3.4×10^{-2}	-1.6×10^{-2}	-8.6×10^{-3}
151	-1.0	1.0	-6.3×10^{-4}	-5.1×10^{-4}	5.1×10^{-8}	4.0×10^{-3}	-1.4×10^{-3}	-6.4×10^{-4}
151	-3.6	1.4	-1.6×10^{-3}	-2.0×10^{-3}	5.4×10^{-7}	1.2×10^{-2}	-4.4×10^{-3}	-2.1×10^{-3}
301	-1.0	1.0	-3.1×10^{-4}	-1.8×10^{-4}	8.1×10^{-9}	2.2×10^{-3}	-5.6×10^{-4}	-2.5×10^{-4}
301	-3.6	1.4	-7.8×10^{-4}	-7.1×10^{-4}	9.0×10^{-8}	6.0×10^{-3}	-1.8×10^{-3}	-8.6×10^{-4}
661	-3.6	1.4	---	2.2×10^{-6}	---	---	-2.6×10^{-4}	---
51	[a]-1.0	[a]1.0	---	---	6.5×10^{-7}	---	---	-2.7×10^{-4}

[a]Nonuniform.

The results of table I show that for a given mesh the best accuracy in the calculation of $\bar{\delta}$ and ΔH is obtained by using the present approach. The value of $\bar{\delta}_{max}$ from Hamrock and Jacobson (ref. 3) is in some cases less accurate than that from Okamura (ref. 4) because they did not use the constant expressed in equation (3). But $\bar{\delta}_{max}$ is not really significant since any inaccuracy in its calculation can be compensated for by H_0 in the film thickness expression. The important parameter of table I is ΔH_{max} since

it is a measure of the flatness of the film shape. This aspect is extremely important at high loads, where the elastic deformations are two or three orders of magnitude larger than the film thickness.

Also shown in table I are the results obtained with a uniform mesh of 661 nodes by Hamrock and Jacobson (ref. 3). Very small values of ΔH_{max} were calculated and cannot be reproduced with the new approach because of storage problems with the matrix D_{ij} and because of the large system of equations that would have to be solved with such a mesh. But using a nonuniform mesh with a fine grid near X equal to -1 and +1 (where 10 subintervals are used in the intervals [-1,-0.96] and [0.96,1]), similar results are found with a very small value of N_{max} (N_{max} = 51), as indicated in table I. The latter case illustrates very well the power of the new approach.

CALCULATION OF dP/dX

The term dP/dX is used to calculate the influence coefficient D_{ij} and is used in the Reynolds equation described later. For the calculation of D_{ij}, $(dP/dX)_i$ at node i is calculated by using three nodes.

$$\left(\frac{dP}{dX}\right)_i = a_{i,i-1}P_{i-1} + a_{i,i}P_i + a_{i,i+1}P_{i+1} \tag{11}$$

where

$$a_{i,i-1} = \frac{X_i - X_{i+1}}{(X_{i-1} - X_i)(X_{i-1} - X_{i+1})} \tag{12}$$

$$a_{i,i} = \frac{2X_i - X_{i+1} - X_{i-1}}{(X_i - X_{i-1})(X_i - X_{i+1})} \tag{13}$$

$$a_{i,i+1} = \frac{X_i - X_{i-1}}{(X_{i+1} - X_{i-1})(X_{i+1} - X_i)} \tag{14}$$

At the first and last nodes, X_1 and $X_{N_{max}}$, dP/dX is also defined by using three nodes (X_1 to X_3 and X_{N-2} to $X_{N_{max}}$).

For the calculation of dP/dX in the Reynolds equation, two nodes may often be used if the numerical convergence is difficult to obtain with the three-node formula. For the two-node formula the weighting factors are

$$a_{i,i+1} = \frac{1}{X_{i+1} - X_i}; \quad a_{i,i} = -a_{i,i+1}; \quad a_{i,i-1} = 0 \tag{15}$$

Minor corrections are also applied on the last values of $a_{n,j}$ to respect the boundary conditions at $X = X_{end}$ and are described in appendix B.

FORMULATION OF MATHEMATICAL PROBLEM

The basic equation to solve in dimensionless form at each node i is the dimensionless Reynolds equations.

$$f_i = H_i^3 \left(\frac{dP}{dX}\right)_i - K\bar{\eta}_i \left(H_i - \frac{\bar{\rho}_e H_e}{\bar{\rho}_i}\right) = 0 \tag{16}$$

with

$$H_i = H_0 + \frac{X_i^2}{2} + \sum_{j=1}^{N} D_{ij} P_j \tag{17}$$

$$\bar{\rho}_i = 1 + \frac{0.6\times10^{-9}\, p_H P_i}{1 + 1.7\times10^{-9}\, p_H P_i} \tag{18}$$

$$\bar{\eta}_i = \exp(\alpha p_H P_i) \qquad \text{if Barus' viscosity is used} \tag{19}$$

$$\bar{\eta}_i = \exp\left\{[\ln(\eta_0) + 9.67][-1 + (1 + 5.1\times10^{-9} p_H P_i)^Z]\right\}$$
$$\text{if Roeland's viscosity is used} \tag{20}$$

$$K = \frac{3}{4}\pi^2 \frac{U}{W^2} \tag{21}$$

where H_0 contains the term $-\ln(8WR^2/\pi)/4$ introduced in equation (3). The parameter Z in Eq. (20) can be expressed in terms of α and η_0 as in reference 6. Furthermore, the constant load is also introduced by

$$\int_{X_{min}}^{X_{end}} P\, dX = \frac{\pi}{2} \tag{22}$$

The unknowns is this problem are

X_{end} outlet meniscus distance defined in figure 1

N number of nodes to use as defined in figure 1

H_0 constant to define

$\bar{\rho}_e H_e$ value of $\bar{\rho}H$ where $dP/dX = 0$

P_j pressure at node j (j = 2, N)

The boundary conditions are

$$P_1 = 0 \quad \text{for} \quad X_1 = X_{min} \tag{23}$$

$$P = dP/dX = 0 \quad \text{for} \quad X = X_{end} \tag{24}$$

Figure 1 illustrates the calculation of X_{end} and N, where X_N is the nearest node to X_{end} such that $X_N < X_{end}$; $H(X)$ can be defined as a second-degree curve using H_{N-1}, H_N, and H_{N+1}; and X_{end} is calculated such that $H(X_{end}) = \bar{\rho}_e H_e$. Having defined X_{end} and N, the remaining $N + 1$ unknowns $\bar{\rho}_e H_e$, H_0, and P_2 to P_N are calculated by using an iterative Newton-Raphson scheme. If the superscripts n and o are used to define the new and old values of the unknowns corresponding to two successive interations, we have

$$(\bar{\rho}_e H_e)^n = (\bar{\rho}_e H_e)^o + [\Delta(\bar{\rho}_e H_e)]^n \tag{25}$$

$$P_j^n = P_j^o + (\Delta P_j)^n \tag{26}$$

$$H_0^n = H_0^o + (\Delta H_0)^n \tag{27}$$

where $[\Delta(\bar{\rho}_e H_e)]^n$, $[\Delta(P_j)]^n$, and $[\Delta(H_0)]^n$ are now the unknowns to the problem. They must all be small if the convergence is obtained. For the data presented, an accuracy of 1/1000 was required on each unknown. From the definition of the Newton-Raphson algorithm, we have for each node i

$$\left[\frac{\partial f_1}{\partial(\bar{\rho}_e H_e)}\right]^o [\Delta(\bar{\rho}_e H_e)]^n + \sum_{j=2}^{N}\left(\frac{\partial f_1}{\partial P_j}\right)^o (\Delta P_j)^n + \left(\frac{\partial f_1}{\partial H_0}\right)^o (\Delta H_0)^n = - f_1^o \tag{28}$$

where $[\partial f_1/\partial(\bar{\rho}_e H_e)]^o$, $(\partial f_1/\partial P_j)^o$, and $(\partial f_1/\partial H_0)^o$ are defined analytically in appendix C. The constant load is taken into account by writing

$$\int_{X_{min}}^{X_{end}} (\Delta P)^n \, dX = \frac{\pi}{2} - \int_{X_{min}}^{X_{end}} P^o \, dX = (\Delta W)^n$$

or (29)

$$\sum_{j=2}^{N} C_j \, (\Delta P_j)^n = (\Delta W)^n$$

where C_j are the weighting factors defined in appendix D. Since X_N does not coincide with X_{end}, minor corrections are applied on the last values of C_j, as described in appendix B. A linear system of $N + 1$ equations is therefore to be solved

$$\begin{bmatrix} \frac{\partial f_1}{\partial(\bar{\rho}_e H_e)} & \frac{\partial f_1}{\partial P_2} & \cdots\cdots & \frac{\partial f_1}{\partial P_N} & \frac{\partial f_1}{\partial H_0} \\ \frac{\partial f_2}{\partial(\bar{\rho}_e H_e)} & \frac{\partial f_2}{\partial P_2} & \cdots\cdots & \frac{\partial f_2}{\partial P_N} & \frac{\partial f_2}{\partial H_0} \\ & & & & \\ \frac{\partial f_N}{\partial(\bar{\rho}_e H_e)} & \frac{\partial f_N}{\partial P_2} & \cdots\cdots & \frac{\partial f_N}{\partial P_N} & \frac{\partial f_N}{\partial H_0} \\ 0 & C_2 & \cdots\cdots & C_N & 0 \end{bmatrix}^o \begin{Bmatrix} \Delta(\bar{\rho}_e H_e) \\ \Delta(P_2) \\ \\ \Delta(P_N) \\ \Delta(H_0) \end{Bmatrix}^n = \begin{Bmatrix} -f_1 \\ -f_2 \\ \\ -f_N \\ \Delta W \end{Bmatrix}^o$$

A Gauss elimination with a partial pivoting method is used to solve this linear system.

RESULTS AND DISCUSSION

The results of employing these techniques are shown in figures 2 to 3. Most of these results have been obtained by using a two-node formulation for dP/dX because the convergence was found to be easier.

Figure 2 gives the pressure profiles and film shapes at iterations 0, 1, and 14. The 14th iteration is the converged solution. Barus' pressure-viscosity expression was used and $W = 2.0452 \times 10^{-5}$, $U = 1.0 \times 10^{-11}$, and $G = 5007$. Barus' viscosity was used as this stage to enable direct comparison with the results of Hamrock and Jacobson (ref. 3). Starting with a Hertzian pressure profile (iteration 0), the present approach converged quickly. At the first iteration a pressure spike was formed that was close to the final converged spike. The initial film level (iteration 0) was obtained from Hamrock and Jacobson (ref. 3). In general, it took about 15 iterations to obtain a converged solution, or about 2 min of CPU time on the IBM 370 computer with a mesh of 181 nodes. Contrast this with the 100 min normally taken by the Hamrock and Jacobson approach. At high loads iterations have to be performed by starting from a previous pressure profile obtained at a lower load.

Figure 3 shows the effects of a number of uniform nodes on H_{min}, H_e, and the pressure spike P_s. The parameters W, U, and G were exactly the same as those described for figure 2, and Barus' viscosity was also used. The actual pressure profiles and film shapes for four nodes are shown at the top of figure 3. The value of H_{min} did not change much as the number of nodes N_{max} increased: H_{min} for $N_{max} = 51$ was about the same as H_{min} for $N_{max} = 321$. With increasing number of nodes H_e approached an asymptotic value. For this case little change was observed when N_{max} became larger than 221. When the three-node formulation of dP/dX was used, the convergence was more difficult to obtain, but some successful runs clearly indicated that considerably fewer nodes were required for a given accuracy of H_e.

The value of the pressure spike fluctuated, especially at low values of N_{max}, because of the position of the nodes relative to the position of the spike. For example, at $N_{max} = 51$ the spike did not develop because of the large spacing of the nodes (sketch at top of fig. 3). Another example is given by the asterisk in figure 3, for $N_{max} = 241$. This asterisk corresponds to the value of P_s when a translation of half an interval has been imposed on the mesh and gives a range of fluctuation of P_s. Note that an increase of 20 was chosen for N_{max} and that more oscillations in P_s might have been found if N_{max} would have been varied more slowly. As the number of nodes was increased, the spike became better defined. At $N_{max} = 261$ the value of P_s started to become stable, although it was still slightly increasing as N_{max} increased. It can therefore be concluded that the amplitude of the spike is limited once a sufficient number of nodes have been used. As the number of nodes increased, there could also be large changes in the pressure spike but little corresponding change in the film thickness. The results presented in figure 3 are for a given uniform mesh. When a nonuniform mesh was used with many nodes near the spike, the pressure spike became better defined.

Hamrock and Jacobson's (ref. 3) and the present film shapes and pressure profiles are compared in figure 4. Parameters were identical to those described for figures 2 and 3, and N_{max} was fixed at 321. The value of H_e as calculated in reference 3 is about 2 percent larger than the value calculated in the present approach; the value of H_{min} is about 9 percent smaller. The pressure spikes also differ in amplitude and position. Although the differences are not yet explained, they could be attributed to the fact that Hamrock and Jacobson were solving the second-order differential Reynolds equation, whereas the present approach solved the first-order differential Reynolds equation. Furthermore, as noted previously, elasticity calculations also differ. The present results are believed to be more accurate than those described in reference 3, where in front of the pressure spike region the sign of dP/dX was not equal to the sign of $(\rho H - \rho_e H_e)$. Furthermore, the mesh flow was not constant in reference 3, whereas the first-order differential Reynolds equation solved in the present approach is directly representative of a constant flow.

Figure 5 shows the pressure profile and the film thickness ratio H/H_e for five dimensionless loads varying over two orders of magnitude (from 2×10^{-5} to 3×10^{-3}). This dimensionless load range corresponds to a maximum Hertzian pressure of 0.4 to 4.8 GPa. A nonuniform mesh was always used in the spike and inlet regions for the high-load cases. For those results Roelands' pressure-viscosity formula was used, and the dimensionless speed and materials parameters were fixed at $U = 1 \times 10^{-11}$ and $G = 5007$. As the load increased (fig. 5(a)), the spike became smaller and moved toward the outlet. Furthermore, as the load increased, the inlet meniscus moved toward the abscissa $X = -1$. The nip film thickness width and length (fig. 5(b)) both decreased as the load increased. This effect could be used to predict, from experimental observations of the nip, the existence and amplitude of the pressure spike.

Figure 6 shows the effect of the dimensionless load W on H_e, H_{min}, and P_s. Conditions were similar to the ones defined in figure 5. At low loads H_{min} was smaller than H_e, but at high loads the reverse was true. The slopes of the curves plotted on a log-log scale are -1.16 for H_e and -1.11 for H_{min}. The slope of H_{min} is similar to the one found by Hamrock and Jacobson in reference 3 where a slope of -0.11 was found when plotting h_{min}/R

versus W. As the load increased, the height of the spike decreased until $W = \sim 3 \times 10^{-4}$, where the spike no longer appeared for these given speed and material conditions. With a much finer nodal structure the spike might be observed even at higher loads, but its height would indeed be quite small.

Figure 7 shows the effect on the pressure and film thickness of using Barus' or Roelands' pressure-viscosity expression. The dimensionless load, speed, and materials parameters were held fixed at $W = 2.0452 \times 10^{-5}$, $U = 1 \times 10^{-11}$, and $G = 5007$. A uniform mesh of 321 nodes extending from -4 to 1.3 was used. The large number of nodes was used to reduce the possibility of spike height instabilities. Barus' formula produced a higher spike and a larger film thickness than Roelands' formula. The increase in H_e was about 3 percent.

Figure 8 shows the effect of lubricant compressibility on film thickness. The parameters U and G were held fixed while W was equal to 3×10^{-3}. In the compressible case the film thickness H_e was reduced by the average density ratio, and H_{min} was larger than H_e. This result is due to the effects of compressibility since in the incompressible case H_{min} was smaller than H_e, as would be expected in order to keep the mass flow constant at the nip, where dP/dX was large and negative. Note also that the incompressible film shape was very close to the Hertzian shape (except near the nip) because of the high loads.

CONCLUSIONS

The film thicknesses and pressures in elastohydrodynamically lubricated contacts have been calculated for a line contact by using an improved version of Okamura's approach. The new approach allows for lubricant compressibility, the use of Roelands' viscosity, a very general mesh (nonconstant step), and very accurate calculations of the elastic deformations. The results indicate that the new method is fast and accurate. The accuracy of the film thickness, pressure, and pressure spike is fully controlled by the type of mesh and the number of nodes used. The new approach is not load limited as were previous approaches. Successful runs have been made at a maximum pressure of 4.8 GPa with low CPU times. This approach can be a useful tool in studying rolling bearings and gears. Calculations of the rolling traction force and pressure spike at high loads are now possible and should be of first importance for predicting rolling-bearing friction and fatigue life.

APPENDIX A

CALCULATION OF ELASTIC DEFORMATIONS

The details of evaluating equation (6) are presented in this appendix. The interval $[X_{min}, X_{end}]$ can be divided into small intervals $[X_{j-1}, X_{j+1}]$ so that the deformation $\bar{\delta}_{ij}$ at node i is the sum of all of the small elementary deformations $d\bar{\delta}_{ij}$ calculated at node i and due to the pressure defined in the interval $[X_{j-1}, X_{j+1}]$.

$$\bar{\delta}_i = \sum_{j=2,4,6....}^{N-1} d\bar{\delta}_{ij} \tag{30}$$

In these small intervals, dP/dX' is assumed to vary linearly with X', and X' varies between $X_{j-1} - X_j$ and $X_{j+1} - X_j$ as indicated on figure 9. When these small intervals are used, the distance $X_i - X_j$, rather than simply X_i, has to be introduced.

$$d\bar{\delta}_{ij} = -\frac{1}{2\pi} \int_{X_{j-1}-X_j}^{X_{j+1}-X_j} \frac{dP}{dX'} (X_i - X_j - X') \left[\ln(X_i - X_j - X')^2 - 2\right] dX' + \text{constant} \tag{31}$$

The linear expression for dP/dX' reads

$$\frac{dP}{dX'} = (a_1X' + a_2)\, P_{j-1} + (a_3X' + a_4)\, P_j + (a_5X' + a_6)\, P_{j+1} \tag{32}$$

where

$$
\left.
\begin{aligned}
a_1 &= \frac{2}{d_1} \\
a_2 &= \frac{-(X_j + X_{j+1})}{d_1} + a_1 X_j \\
d_1 &= (X_{j-1} - X_j)(X_{j-1} - X_{j+1}) \\
a_3 &= \frac{2}{d_2} \\
a_4 &= \frac{-(X_{j+1} + X_{j-1})}{d_2} + a_3 X_j \\
d_2 &= (X_j - X_{j-1})(X_j - X_{j+1}) \\
a_5 &= \frac{2}{d_3} \\
a_6 &= \frac{-(X_j + X_{j-1})}{d_3} + a_5 X_j \\
d_3 &= (X_{j+1} - X_{j-1})(X_{j+1} - X_j)
\end{aligned}
\right\} \qquad (33)
$$

From the expression for dP/dX', it can be seen that $d\bar{\delta}_{1j}$ can be expressed as

$$d\bar{\delta}_{1j} = dD_{1,j-1}P_{j-1} + dD_{1,j}P_j + dD_{1,j+1}P_{j+1} + \text{constant} \qquad (34)$$

where $dD_{1,j}$ are the elementary influence coefficients calculated as

$$dD_{1,j-1} = -\frac{1}{2\pi}\int_{X_{j-1}-X_j}^{X_{j+1}-X_j} (a_1X' + a_2)(X_1 - X_j - X')\left[\ln (X_1 - X_j - X')^2 - 2\right] dX' \qquad (35)$$

A similar relation that uses the corresponding coefficients a_3, a_4 and a_5, a_6 is used to define $dD_{1,j}$ and $dD_{1,j+1}$. By adopting the change of variables

$$
\left.
\begin{aligned}
Z = X_1 - X_j - X';\ Z_{min} = X_1 - X_{j-1};\ Z_{max} = X_1 - X_{j+1} \\
b_2 = a_1(X_1 - X_j) + a_2;\quad dZ = -dX'
\end{aligned}
\right\} \qquad (36)
$$

$dD_{1,j-1}$ is calculated as

$$dD_{i,j-1} = -\frac{1}{2\pi}\int_{Z_{min}}^{Z_{max}} -(-a_1 Z + b_2)\, Z \left[\ln (Z^2) - 2\right] dZ$$

$$= -\frac{1}{2\pi}\left[-b_2 \int_{Z_{min}}^{Z_{max}} Z \ln Z\, dZ + a_1 \int_{Z_{min}}^{Z_{max}} Z^2 \ln Z^2\, dZ + 2b_2 \right.$$

$$\left. \times \left| \frac{Z^2}{2} \right|_{Z_{min}}^{Z_{max}} - 2a_1 \left| \frac{Z^3}{3} \right|_{Z_{min}}^{Z_{max}} \right]$$

$$= -\frac{1}{2\pi}\left| -2b_2 \frac{Z^4}{4} (\ln Z^2 - 1) + 2a_1 \frac{Z^3}{9}\left(\ln |Z|^3 - 1\right) + 2b_2 \frac{Z^2}{2} - 2a_1 \frac{Z^3}{3} \right|_{Z_{min}}^{Z_{max}} \tag{37}$$

Using the variables M, N, and K, we obtain after rearrangement

$$\left.\begin{aligned} dD_{i,j-1} &= -\frac{1}{2\pi}\left(a_1 K + a_2 \frac{M}{2}\right) \\ dD_{i,j} &= -\frac{1}{2\pi}\left(a_3 K + a_4 \frac{M}{2}\right) \\ dD_{i,j+1} &= -\frac{1}{2\pi}\left(a_5 K + a_6 \frac{M}{2}\right) \end{aligned}\right\} \tag{38}$$

where

$$\left.\begin{aligned} M &= Z_{min}^2 \left(\ln Z_{min}^2 - 3\right) - Z_{max}^2 \left(\ln Z_{max}^2 - 3\right) \\ N &= Z_{max}^3 \left(\ln |Z_{max}|^3 - 4\right) - Z_{min}^3 \left(\ln |Z_{min}|^3 - 4\right) \\ K &= M \frac{X_i - X_j}{2} + \frac{2N}{9} \end{aligned}\right. \tag{39}$$

There is no problem concerning the singularity occurring for $X_i = X_j$. When there is a singularity in the interval $[X_{i-1}, X_{i+1}]$, we can integrate along the two half intervals $[X_{i-1}, X_i]$ and $[X_i, X_{i+1}]$ and use the relation

$$\lim_{Z\to 0} (Z^2 \ln Z^2) = \lim_{Z\to 0} (Z^3 \ln |Z|^3) = 0 \tag{40}$$

which shows the relations (38) to be also valid for $X_1 = X_j$. Finally, the deformation $\bar{\delta}_1$ is obtained by summing all of the elementary small deformations $d\bar{\delta}_{1j}$

$$\bar{\delta}_1 = \sum_{j=2,4,6,\ldots}^{N-1} d\bar{\delta}_{1,j} \tag{41}$$

$$\bar{\delta}_1 = \sum_{j=1}^{N} D_{1,j} P_j - \frac{1}{4} \ln \left(R^2 \frac{8W}{\pi} \right) \tag{42}$$

where $D_{1,j} = dD_{1,j}$ if j is even. If j is odd ($j = 3$ in the following example), we calculate dD_{13} coming from the interval $[X_1, X_3]$ and add to it the value dD_{1j} coming from the interval $[X_3, X_5]$ in order to obtain the final value of D_{13}. For the first and last values of $D_{1,j}$, we simply have

$$\begin{aligned} D_{1,1} &= dD_{1,1} \\ D_{1,N} &= dD_{1,N} \end{aligned} \tag{43}$$

Note now that $\sum_j D_{1,j} P_j$ is independent of the load. At high loads the dimensionless film thickness H_e becomes very small with respect to $\bar{\delta}_1$. However, by using an appropriate change of variable ($X = x/bc$), the maximum deformation $\bar{\delta}_{max}$ can be kept equal to H_e. Using the last change of variable, we have

$$\bar{\delta}_1 = c \sum_{j=1}^{N} D'_{1j} P_j - \frac{1}{4} \ln \left(R^2 \frac{8W}{\pi} c^2 \right) \tag{44}$$

where D'_{1j} are the new influence coefficients obtained with the new value of X. From the definition of c we have

$$c \sum D'_{1j} P_j = H_e \tag{45}$$

The maximum deformation $\bar{\delta}_{max}$ is close to the maximum Hertzian deformation $\bar{\delta}_H$ (defined in eq. (10)), leading to

$$-\frac{1}{4} \ln \left(R^2 \frac{8W}{\pi} \right) + \frac{1}{2} \ln 2 + \frac{1}{4} = H_e - \frac{1}{4} \ln \left(R^2 \frac{8W}{\pi} c^2 \right) \tag{46}$$

The value of c can therefore be defined as

$$c = \frac{1}{2} \exp (2H_e - 0.5) \tag{47}$$

This numerical "trick" was definitively helpful at high loads but was not used in the results presented herein.

APPENDIX B

CORRECTIONS TO BE APPLIED TO WEIGHTING FACTORS DUE TO X

For $X = X_{end}$, $P = dP/dX = 0$. It is assumed that between X_N and X_{end}, $P(X)$ is described by a second-degree polynomial. To respect the previously mentioned boundary condition, we have

$$P = \frac{(X - X_{end})^2}{(X_N - X_{end})^2} P_N \tag{48}$$

$$\frac{dP}{dX} = \frac{2(X - X_{end})}{(X_N - X_{end})^2} P_N \tag{49}$$

For $X = X_N$ we have therefore

$$\left(\frac{dP}{dX}\right)_N = \frac{2}{X_N - X_{end}} P_N \tag{50}$$

which can also be expressed as

$$a_{n,n-1} = 0; \quad a_{n,n} = \frac{2}{X_N - X_{end}}; \quad a_{n,n+1} = 0 \tag{51}$$

The integral of the pressure between X_N and X_{end} leads to

$$\int_{X_N}^{X_{end}} P \, dX = \frac{1}{3} [X_{end} - X_N] P_N = \Delta C_N P_N \tag{52}$$

If N is odd, we substract from the value of C_N the value $dC_{N+1,N}$ coming from the interval $[X_N, X_{N+2}]$ and add ΔC_N to set the final value of C_N. If N is even, we modify C_{N-1} and C_N. From C_{N-1}, we substract $dC_{N,N-1}$ from the interval $[X_{N-1}, X_{N+1}]$ and add the weighting factor ΔC_{N-1} coming from the integration of P between X_{N-1} and X_N. Using the "trapeze" rule,

$$\Delta C_{N-1} = \frac{X_N - X_{N-1}}{2} \tag{53}$$

The value of C_N is finally defined as

$$C_N = \Delta C_{N-1} + \Delta C_N \tag{54}$$

APPENDIX C

CALCULATION OF JACOBIAN FACTORS

The factors to be defined are

$$\frac{\partial f_i}{\partial(\bar{\rho}_e H_e)}; \quad \frac{\partial f_i}{\partial P_j}; \quad \frac{\partial f_i}{\partial H_0}$$

with

$$f_i = H_i^3 \left(\frac{dP}{dX}\right)_i - K\bar{n}_i \left(H_i - \frac{\bar{\rho}_e H_e}{\bar{\rho}_i}\right) \tag{16}$$

$$H_i = H_0 + \frac{X_i^2}{2} + \sum_{j=1}^{N} D_{ij} P_j \tag{17}$$

dP/dX, $\bar{n}_i$, and $\bar{\rho}_i$ are defined by equations (11), (19) or (20), and (18). Before the final Jacobian factors are defined, we can define

$$\left.\begin{aligned}
&\frac{\partial H_i}{\partial H_0} = 1; \qquad \frac{\partial H_i}{\partial P_j} = D_{ij} \\
&\frac{\partial \bar{n}_i}{\partial P_j} = \alpha p_H \bar{n}_i k_{ij} \qquad \text{if Barus' viscosity is used} \\
&\frac{\partial n_i}{\partial P_j} = 5.1\times10^{-9}\, p_H\, (\ln n_0 + 9.67)(1 + 5.1\times10^{-9} p_H P_i)^{Z-1}\, \bar{n}_i k_{ij} \\
&\qquad\qquad \text{if Roelands' viscosity is used} \\
&\text{where } k_{ij} \text{ is the Kronecker symbol } (k_{ij} = 1 \text{ if } i = j;\ = 0 \text{ if } i \neq j) \\
&\frac{\partial(1/\bar{\rho}_i)}{\partial P_j} = -\frac{0.6\times10^{-9}\, p_H}{1 + 2.3\times10^{-9}\, p_H P_i} k_{ij} \\
&\frac{\partial\left[\left(\frac{dP}{dX}\right)_i\right]}{\partial P_j} = a_{i,i-1} k_{i-1,j} + a_{ii} k_{ij} + a_{i,i+1} k_{i+1,j}
\end{aligned}\right\} \tag{55}$$

It is now easy to define the Jacobian factors

$$\frac{\partial f_1}{\partial(\bar{\rho}_e H_e)} = \frac{K\bar{n}_1}{\bar{\rho}_1}$$

$$\frac{\partial f_1}{\partial P_j} = 3H_1^2 \left(\frac{dP}{dX}\right)_1 D_{1j} + H_1^3 \frac{\partial\left[\left(\frac{dP}{dX}\right)_1\right]}{\partial P_j} - K \frac{\partial \bar{n}_1}{\partial P_j}\left(H_1 - \frac{\bar{\rho}_e H_e}{\bar{\rho}_1}\right) \qquad (56)$$

$$- Kn_1 \left[D_{1j} - \bar{\rho}_e H_e \frac{\partial\left(\frac{1}{\bar{\rho}_1}\right)}{\partial P_j}\right]$$

$$\frac{\partial f_1}{\partial H_0} = 3H_1^2 \left(\frac{dP}{dX}\right)_1 - K\bar{n}_1$$

APPENDIX D

DEFINITION OF WEIGHTING FACTORS C_j

The weighting factors C_j are defined by using the three-point Lagrange polynomial with a general mesh (nonconstant step). In the interval $[X_{j-1}, X_{j+1}]$ the pressure is described by a second-degree polynomial in X'

$$P = \frac{X'(X' + X_j - X_{j+1})}{(X_{j-1} - X_j)(X_{j-1} - X_{j+1})} P_{j-1} + \frac{(X' + X_j - X_{j-1})(X' + X_j - X_{j+1})}{(X_j - X_{j-1})(X_j - X_{j+1})} P_j + \frac{(X' + X_j - X_{j-1})\, X'}{(X_{j+1} - X_{j-1})(X_{j+1} - X_j)} P_{j+1} \tag{57}$$

We can now define the coefficients $dC_{j,j-1}$, dC_{jj}, and $dC_{j,j+1}$ such that

$$\int_{X'_{min}}^{X'_{max}} P\, dX' = dC_{j,j-1} P_{j-1} + dC_{jj} P_j + dC_{j,j+1} P_{j+1}$$

$$\text{with } X'_{min} = (X_{j-1} - X_j);\ X'_{max} = (X_{j+1} - X_j) \tag{58}$$

$$\left.\begin{aligned} dC_{j,j-1} &= \frac{1}{(X_{j-1} - X_j)(X_{j-1} - X_{j+1})} \left| \frac{X'^3}{3} + (X_j - X_{j+1}) \frac{X'^2}{2} \right|_{X'_{min}}^{X'_{max}} \\ dC_{j,j} &= \frac{1}{(X_j - X_{j-1})(X_j - X_{j+1})} \left| \frac{X'^3}{3} + (2X_j - X_{j-1} - X_{j+1}) \frac{X'^2}{2} \right. \\ &\qquad \left. + (X_j - X_{j-1})(X_j - X_{j+1})\, X' \right|_{X'_{min}}^{X'_{max}} \\ dC_{j,j+1} &= \frac{1}{(X_{j+1} - X_{j-1})(X_{j+1} - X_j)} \left| \frac{X'^3}{3} + (X_j - X_{j-1}) \frac{X'^2}{2} \right|_{X'_{min}}^{X'_{max}} \end{aligned}\right\} \tag{59}$$

These coefficients are calculated for $j = 2,4,\ldots, N - 1$. The coefficients C_j are finally defined as

$$C_j = dC_{j,j} \quad \text{if } j \text{ is even}$$

When j is odd ($j = 3$ in the following example), we calculate $dC_{2,3}$ corresponding to the interval $[X_1, X_3]$ and add to it $dC_{4,3}$ coming from the interval $[X_3, X_5]$ in order to define C_j or C_3 in this example. Minor corrections are also applied on the last values of C_j in order to respect the boundary condition for $X = X_{end}$, as shown in appendix B.

REFERENCES

1. Grubin, A.N., and Vinogradova, I.E., "Fundamentals of the Hydrodynamic Theory of Lubrication of Heavily Loaded Cylindrical Surfaces," Investigation of the Contact Machine Components, Kh.F. Ketova, ed., Translation of Russian Book No. 30, Central Scientific Institute of Technology and Mechanical Engineering, Moscow, (Available from Dept. of Scientific and Industrial Research, Great Britain, Transl. CTS-235, and from Special Libraries Association, Chicago, Trans. R-3554), 1949, Chapter 2.

2. Hamrock, B.J. and Tripp, J.H, "Numerical Methods and Computers Used in Elastohydrodynamic Lubrication," Developments in Numerical and Experimental Methods Applied to Tribology: Proceedings of the 10th Leeds-Lyon Symposium on Tribology, Butterworths, Guilford, England, 1984, pp. 11-19.

3. Hamrock, B.J. and Jacobson, B.O., "Elastohydrodynamic Lubrication of Line Contacts,: ASLE Transactions, Vol. 24, No. 4, Oct. 1984, pp. 275-287.

4. Okamura, H., "A Contribution to the Numerical Analysis of Isothermal Elastohydrodynamic Lubrication," Tribology of Reciprocating Engines: Proceedings of the 9th Leeds-Lyon Symposium on Tribology, Butterworths, Guilford, England, 1982, pp. 313-320.

5. Roelands, C.J.A., "Correlational Aspects of the Viscosity-Temperature-Pressure Relationship of Lubricating Oils," Ph.D. Thesis, Technische Hogeschool, Delft, Netherlands, (V.R.B., Groningen, Netherlands) 1966.

6. Houpert, L., "New Results of Traction Force Calculations in Elastohydrodynamic Contacts," ASME Journal of Tribology, Vol. 107, pp. 241-248, 1985.

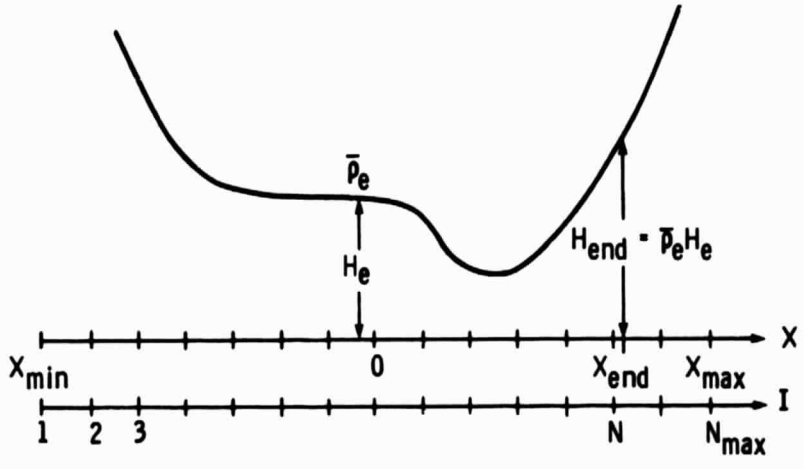

Fig. 1 Sketch to illustrate calculations of X_{end} and N.

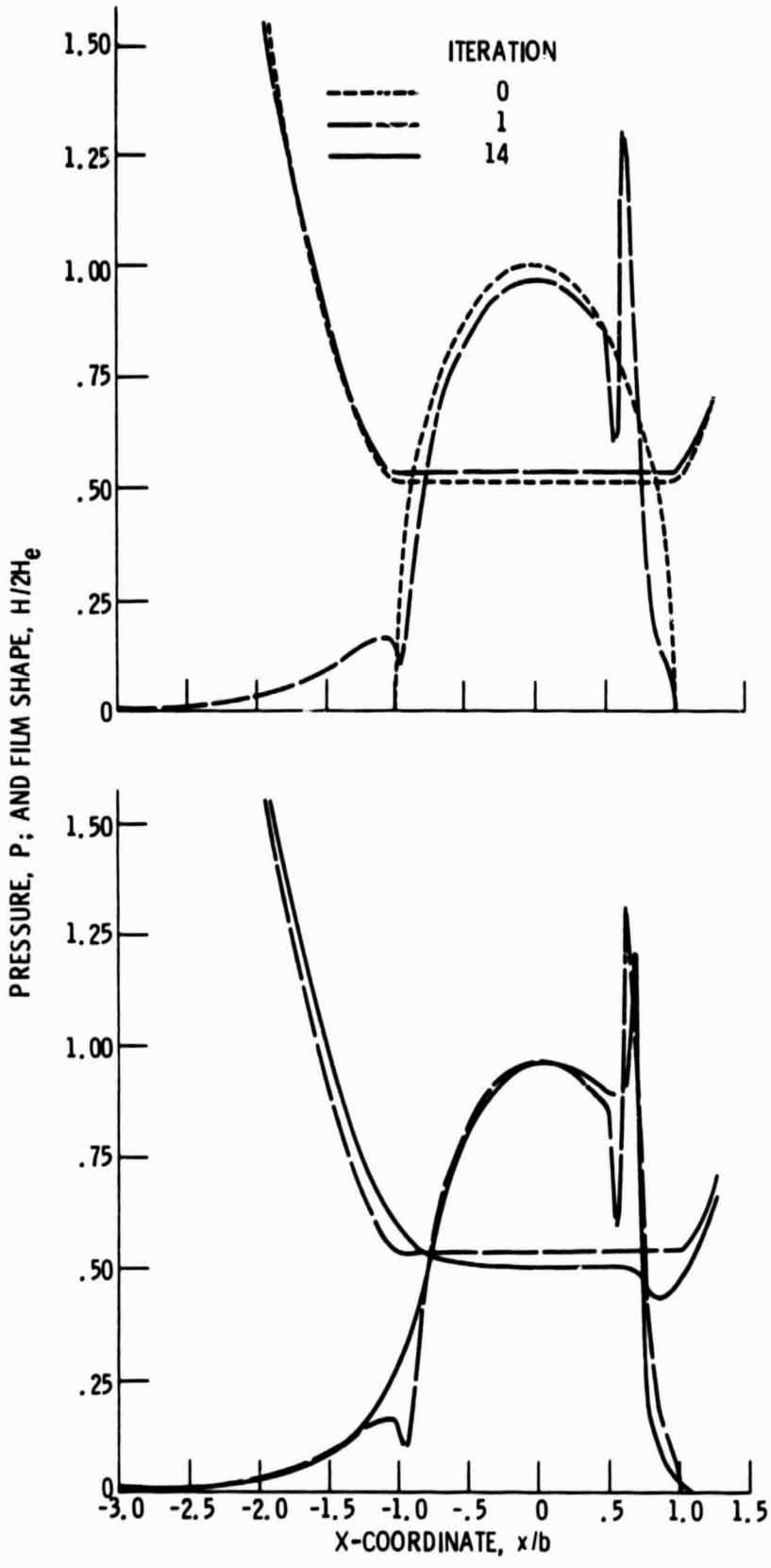

Fig. 2 Pressure profiles and film shapes at iterations 0, 1, and 14. Barus' pressure-viscosity formula; $W = 2.0452 \times 10^{-5}$; $U = 1.0 \times 10^{-11}$; and $G = 5007$.

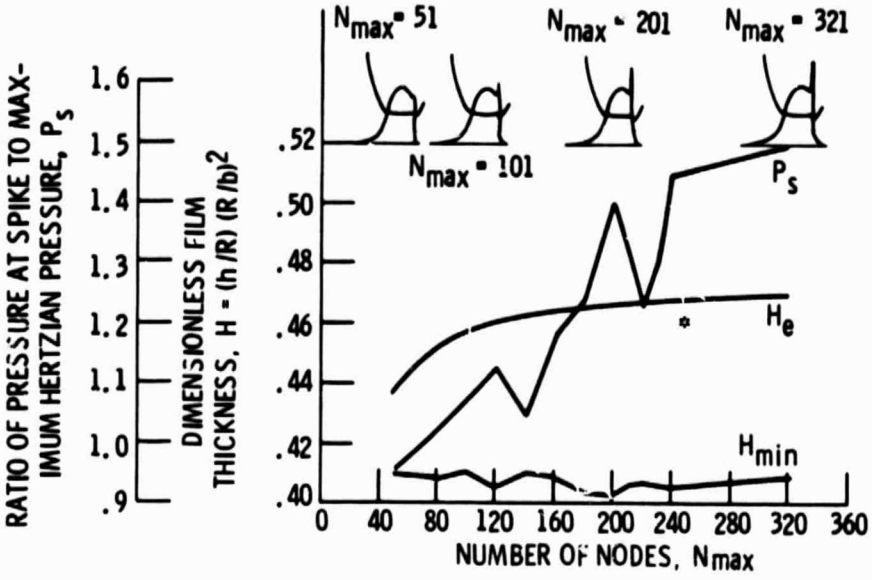

Fig. 3 Effect of number of uniform nodes on H_{min}, H_e, and P_s for a fixed $W = 0.20452 \times 10^{-4}$, $U = 1 \times 10^{-11}$, and $G = 5007$. Barus' pressure-viscosity formula assumed.

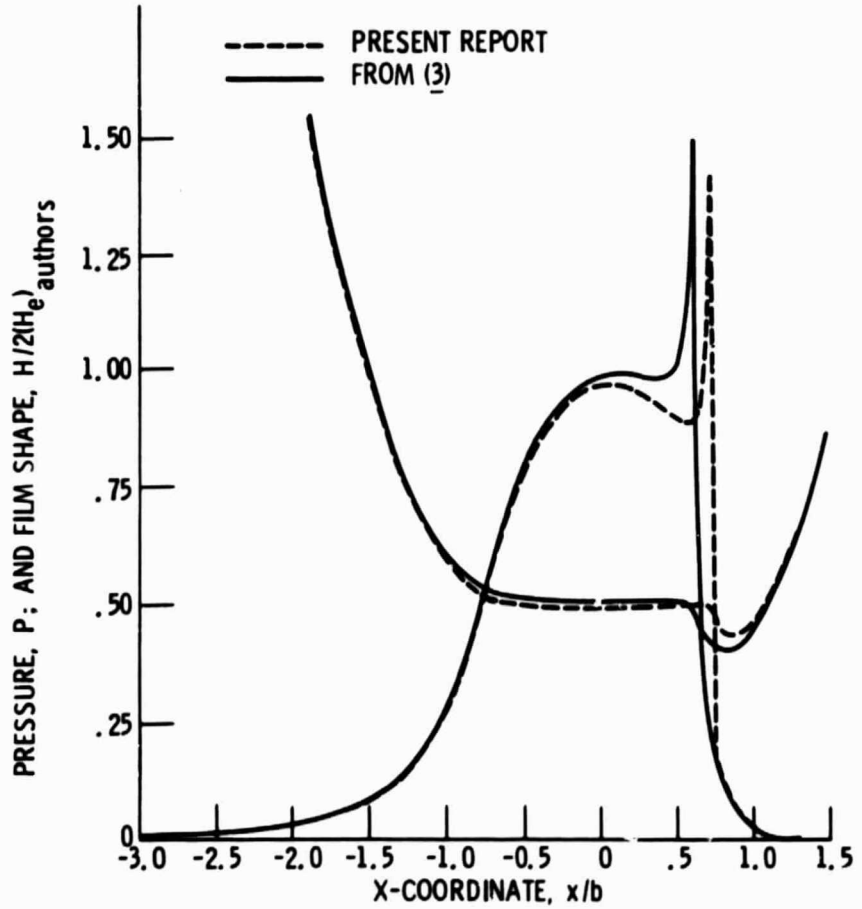

Fig. 4 Comparison between Hamrock and Jacobson's pressure profile and film shape (3) and the authors'. Barus' pressure-viscosity formula; $W = 2.0452 \times 10^{-5}$; $U = 1.0 \times 10^{-11}$; $G = 5007$; and $N_{max} = 321$.

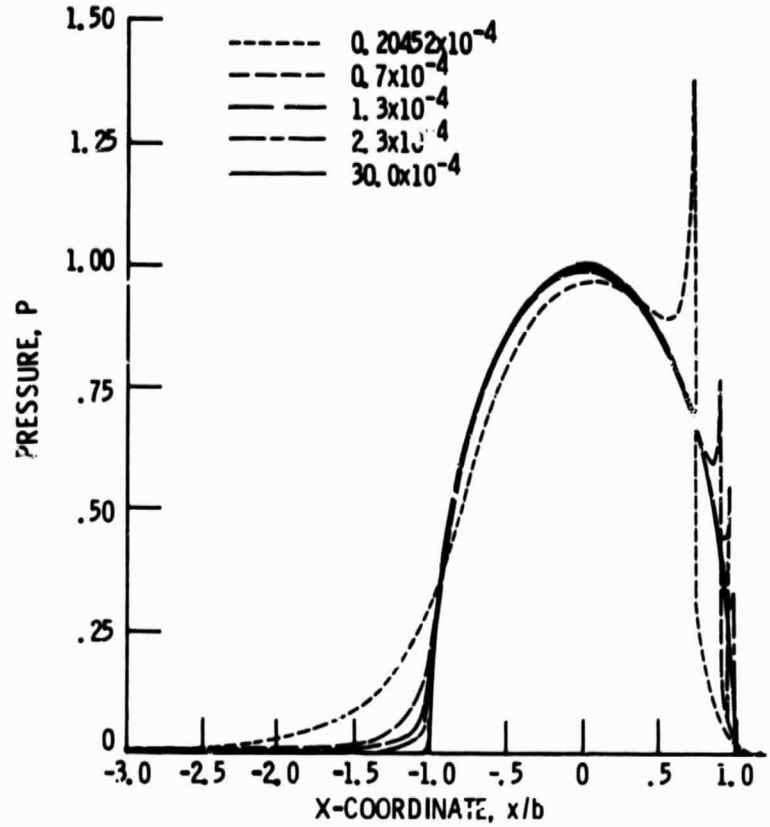

(a) Pressure profiles.

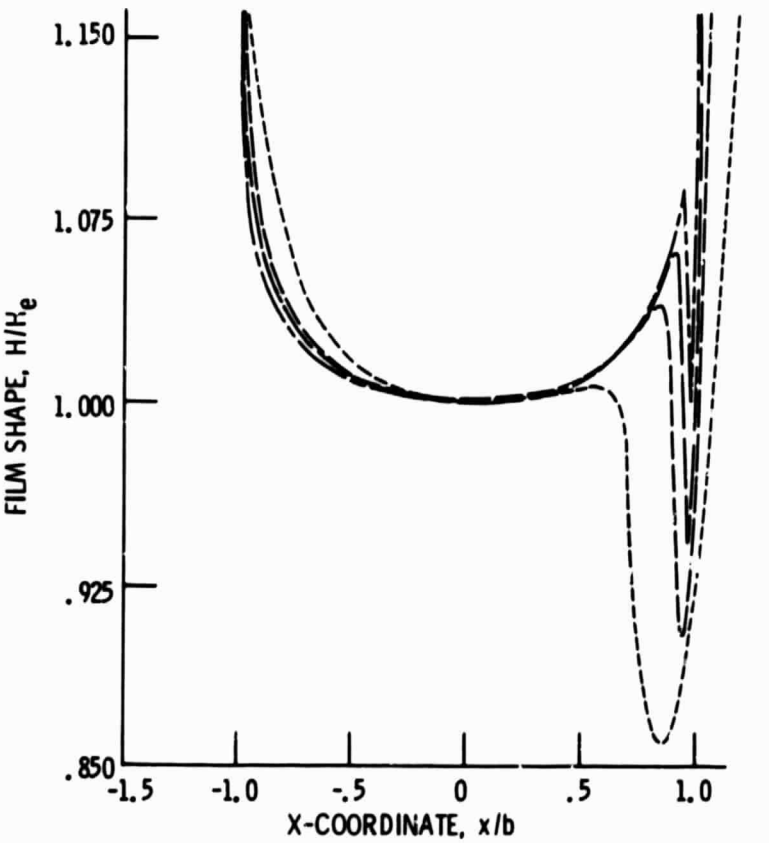

(b) Film shapes.

Fig. 5 Pressure profiles and film shapes for varying dimensionless loads. Roelands' pressure-viscosity formula; $U = 1.0 \times 10^{-11}$; and $G = 5007$.

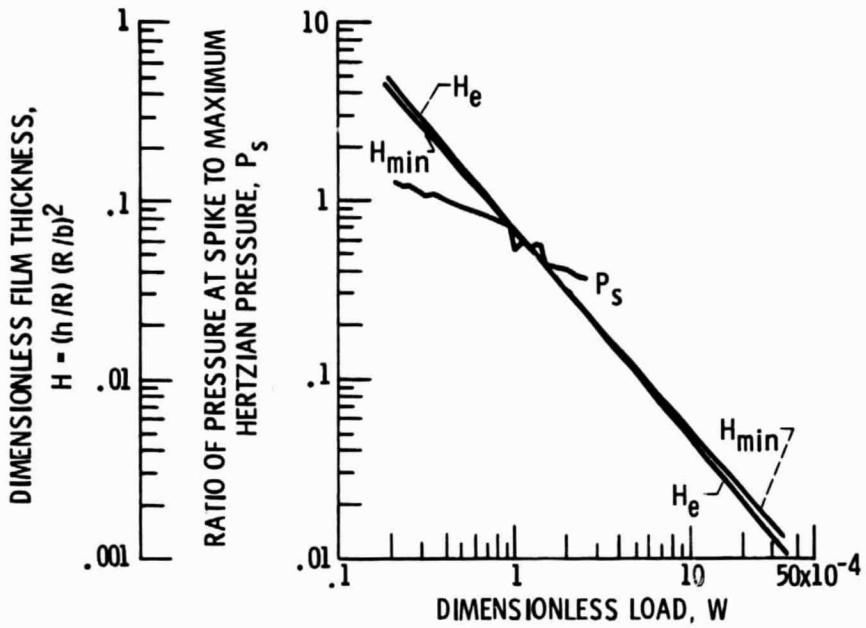

Fig. 6 Effect of dimensionless load W on H_e, H_{min}, and P_s. Roelands' formula for pressure-viscosity assumed; $U = 1.0 \times 10^{-11}$; and $G = 5007$.

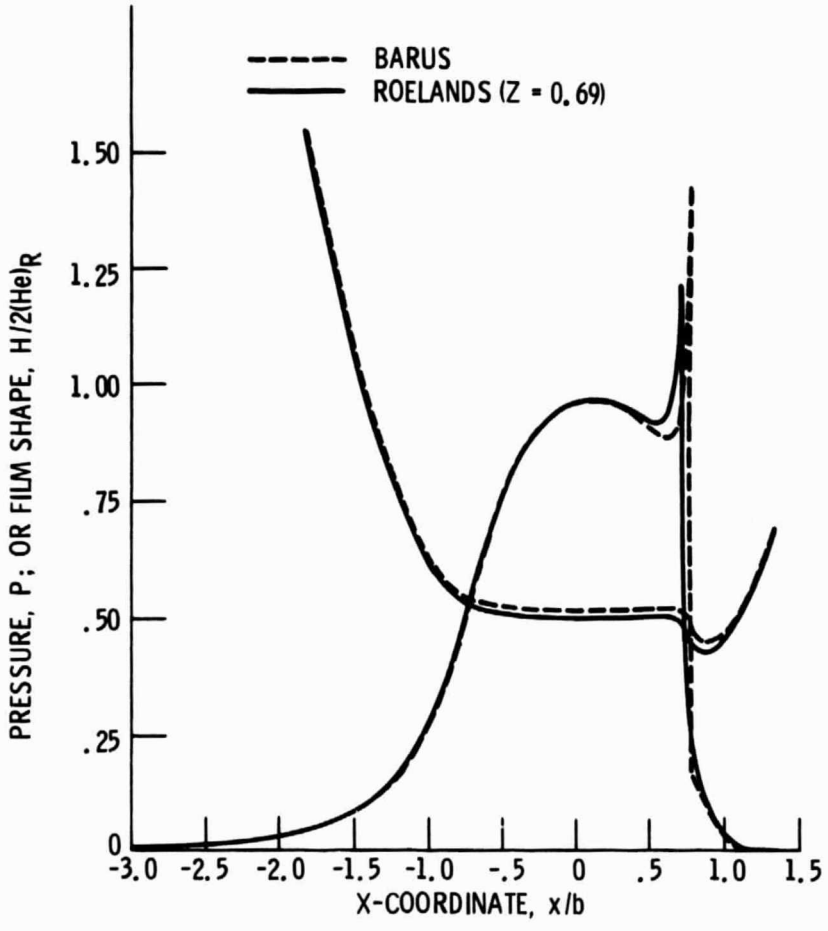

Fig. 7 Effect of using Barus' or Roelands' pressure-viscosity formula on pressure and film shape. Dimensionless load, speed, and materials parameters held fixed at $W = 0.2045 \times 10^{-4}$, $U = 1 \times 10^{-11}$, and $G = 5007$. Uniform mesh of 321 modes extending from X equal -4 to 1.3 used.

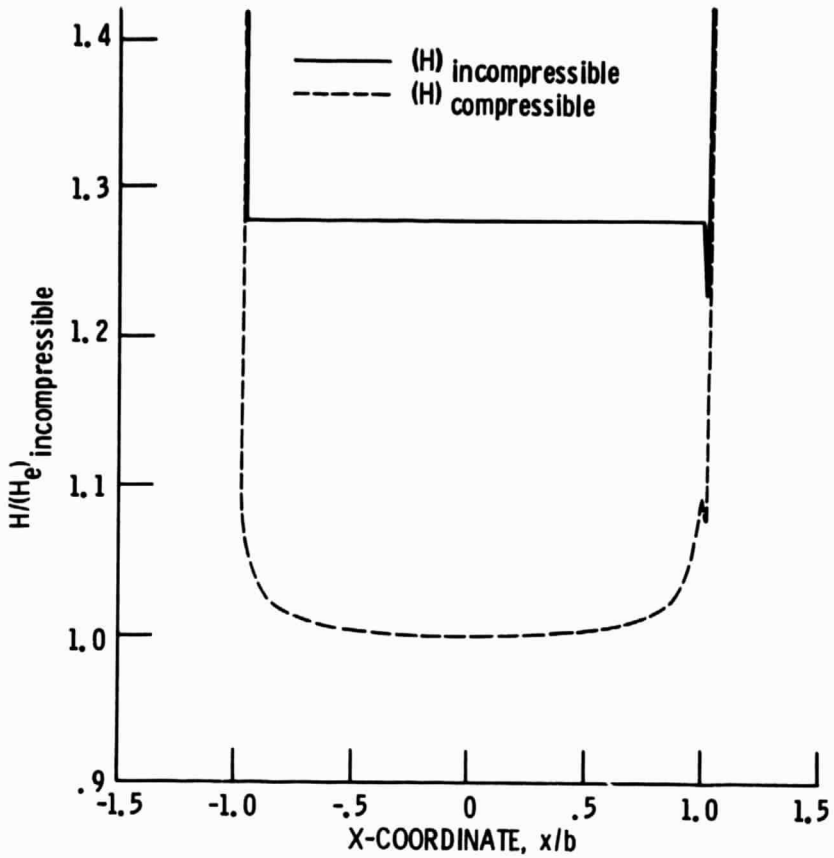

Fig. 8 Effect of lubricant compressibility on film thickness. $U = 1.0 \times 10^{-11}$; $W = 3 \times 10^{-3}$; and $G = 5007$.

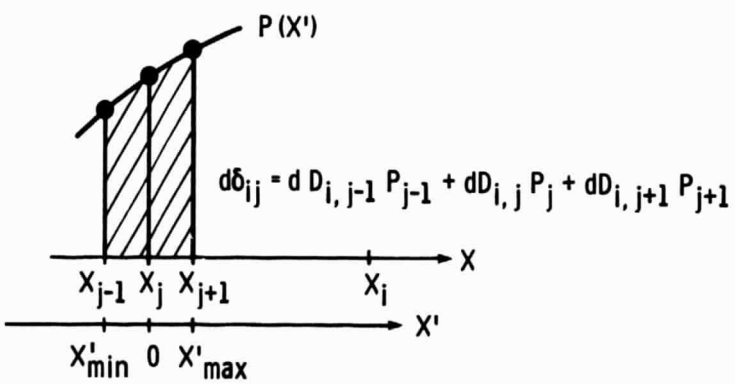

Fig. 9 Calculation of deformation $d\delta_{ij}$ at node i due to pressure acting in interval $[X_{j-1}, X_{j+1}]$.

1. Report No.	2. Government Accession No.	3. Recipient's Catalog No.
NASA TM-87032		

4. Title and Subtitle

Fast Approach for Calculating Film Thicknesses and Pressures in Elastohydrodynamically Lubricated Contacts at High Loads

5. Report Date

6. Performing Organization Code

505-33-62

7. Author(s)

Luc G. Houpert and Bernard J. Hamrock

8. Performing Organization Report No.

E-2581

10. Work Unit No.

9. Performing Organization Name and Address

National Aeronautics and Space Administration
Lewis Research Center
Cleveland, Ohio 44135

11. Contract or Grant No.

13. Type of Report and Period Covered

Technical Memorandum

Sponsoring Agency Name and Address

National Aeronautics and Space Administration
Washington, D.C. 20546

14. Sponsoring Agency Code

15. Supplementary Notes

Luc G. Houpert, presently at S.K.F. Engineering and Research Center, 3430AB Nieuwegein, The Netherlands; NRC-NASA Research Associate during academic year 1984-85. Bernard J. Hamrock, NASA Lewis Research Center. Prepared for the Joint Lubrication Conference, cosponsored by the American Society of Lubrication Engineers and the American Society of Mechanical Engineers, Atlanta, Georgia, October 8-10, 1985.

16. Abstract

The film thicknesses and pressures in elastohydrodynamically lubricated contacts have been calculated for a line contact by using an improved version of Okamura's approach. The new approach allows for lubricant compressibility, the use of Roelands' viscosity, a general mesh (nonconstant step), and accurate calculations of the elastic deformations. The new approach is described, and the effects on film thickness, pressure, and pressure spike of each of the improvements are discussed. Successful runs have been obtained at high pressure (to 4.8 GPa) with low CPU times.

17. Key Words (Suggested by Author(s))	18. Distribution Statement
Elastohydrodynamic contacts High loads	Unclassified - unlimited STAR Category 34

19. Security Classif. (of this report)	20. Security Classif. (of this page)	21. No. of pages	22. Price*
Unclassified	Unclassified		

*For sale by the National Technical Information Service, Springfield, Virginia 22161